Fuel Processing Technology 192 (2019) 75–86

Contents lists available at ScienceDirect

Fuel Processing Technology

journal homepage: www.elsevier.com/locate/fuproc

Research article

Chemical looping gasification of coal using calcium ferrites as oxygen carrier

Yanan Wang[1], Pengjie Niu[1], Haibo Zhao*

State Key Laboratory of Coal Combustion, School of Energy and Power Engineering, Huazhong University of Science and Technology, Wuhan 430074, PR China

ARTICLE INFO

Keywords:
Chemical looping gasification
CaO/Fe_2O_3
Oxygen carrier
Promoting effect
Regulating effect

ABSTRACT

Chemical-looping gasification (CLG) is a novel technology to convert solid fuels like coal and biomass into combustible gases. Without the requirement of high-cost pure oxygen production, CLG utilizes lattice oxygen from oxygen carrier (OC) for partial oxidation of fuels. In this work, the bimetallic CaO/Fe_2O_3 oxygen carriers (OCs) prepared by the wet-impregnation method were tested in a batch fluidized bed reactor using coal (char) as the fuel. The results indicate that increasing CaO addition tends to elevate the low heating value (LHV) of the gas products, and the maximum H_2/CO ratio of 4.6 was attained with coal when FeCa50 (the molar ratio of CaO to Fe_2O_3 is 0.5:0.5) was used as OC. It was found that the char gasification rate is closely dependent on both lattice oxygen donation ability and catalytic activity of OCs. $Ca_2Fe_2O_5$ was determined as a catalytic substance, and the catalytic effect on char gasification was shown to be prominent at the later stage of char gasification when the lattice oxygen donation ability of OCs reduces. Moreover, the catalytic effect of partially reduced OCs on the water-gas shift (WGS) and steam-iron reactions (which may regulate the quality of gas products) was also explored. $Ca_2Fe_2O_5$, with the presence of oxygen vacancies, exhibits better catalytic activity to WGS for attaining higher CO conversion and selectivity, as compared with $CaFe_3O_5$ (moderate catalysis) and Fe_3O_4 (weak catalysis). However, $Ca_2Fe_2O_5$, with a poor reducibility, limits the hydrogen production during the iron-steam process, but it indeed improves the hydrogen production rate owing to its active sites.

1. Introduction

It is urgent to demand efficient, clean, and low-carbon energy technology for the utilization of fossil fuels (especially coal, which is still the main primary energy in China, even in the coming decades). Chemical looping gasification (CLG) is emerging as a novel technology to convert solid fuels (such as coal and biomass) into higher-quality gaseous fuels without the requirement of high-cost pure oxygen production as in conventional gasification technology [1–3]. Indeed, CLG utilizes lattice oxygen provided by oxygen carrier (OC) for partial oxidation of solid fuels (in a fuel reactor). The reduced OC (re-OC) is regenerated in an air reactor, meanwhile a large amount of heat is released. Therefore, OC is also the heat deliverer when circulating between exothermic air reactor and endothermic fuel reactor, in such a way that a large amount of heat needed in the gasification process is factually supplied by the oxidation of re-OC (as well as the combustion of a small amount of carbon residue in a real process), and then autothermal operation is realizable. Obviously, OC plays a key role in the CLG process. The development of high-quality OC (*e.g.*, lattice oxygen carrying capacity and donation ability, resistance to attrition/fragmentation/agglomeration/sintering at high temperatures, non-toxicity, low cost, *etc.*) is one of the main focuses in this field.

By now > 1000 OC materials have been studied for chemical looping applications [4–6]. Single metal oxides or sulfates were considered firstly as the active components in the early development of OC materials. Transition metal oxides such as Fe_2O_3 [7,8], CuO [9,10], NiO [11,12], Mn_2O_3 [13,14], and Co_3O_4 [15,16] have been highly favored due to satisfying thermodynamic properties in the process of reduction and oxidation. Interestingly, a liquid chemical looping gasification concept is proposed by Sarafraz et al. [17,18], and the liquid metal oxide implemented as oxygen carrier can avoid challenges such as agglomeration and sintering that are typically associated with the solid metal oxides. Recent researches have focused on the use of multiple metal-based composite materials for improved and synergistic performance. Wang et al. [19] proposed a novel bimetallic OC, which integrated Cu and Fe metals into one oxide matrix, with superior characteristics over single metal oxide (*e.g.*, higher reactivity than Fe_2O_3, and improved resistance to sintering as compared to CuO [20]). When the Cu−Fe metal oxides used as the OC during the biomass-derived CLG process, it exhibited a high potential to decrease the yield of large molecular compounds and promote the decomposition of small molecular compounds in tar [21].

* Corresponding author.
E-mail address: hzhao@mail.hust.edu.cn (H. Zhao).
[1] Yanan Wang and Pengjie Niu contributed this work equally.

https://doi.org/10.1016/j.fuproc.2019.04.009
Received 9 December 2018; Received in revised form 3 April 2019; Accepted 3 April 2019
Available online 24 April 2019
0378-3820/

With respect to the CLG of coal, the volatiles are firstly released from coal pyrolysis reaction, then char is gasified by CO_2 and/or H_2O. It is well-known that char gasification is the rate-limiting step in comparison with volatiles/gasification products reacting with OC in chemical looping system. The OCs modification by alkali or alkaline earth metal had been proved as an effective method to improve the solid fuel conversion rate [22–24]. Bao et al. [25] investigated the effects of different foreign ions (K^+, Na^+, and Ca^{2+}) on the reduction reactivity of ilmenite and found that the addition of foreign ions significantly promoted the reduction reactivity of ilmenite. Chen et al. [26] used the red mud (a kind of alumina industrial solid waste) as OC to explore its performance in coal char gasification and found that the existence of alkali metal and alkaline earth metal improved the catalytic performance of OC in coal char gasification and water-gas shift (WGS) reaction. Deng et al. [27] proposed that the combination of the two types of red muds (one with rich Fe_2O_3, the other with rich inert and alkaline components) in an appropriate ratio could effectively improve the the activity and stability of the OC than the single ones. CaO has been reported to promote CO_2 sorption and tar cracking in the CLG of biomass [28]. Guo et al. [29] investigated synthesis gas generation from coal CLG using surface Ca-doped iron-based OCs in a fluidized-bed reactor, demonstrating that the addition of CaO increased the carbon conversion efficiency and the gasification rate, and reduced the generation rate of H_2S. Ismail et al. [30,31] reported that the addition of CaO into Fe_2O_3 showed improvements in oxygen carrying capacity, cyclic stability and reactivity over unmodified iron oxide. Additionally, Siriwardane et al. [32] demonstrated that Ca-ferrite and Ba-ferrite presented high reactivity with coal directly *via* solid-solid reaction but low reactivity with synthesis gas, which is very attractive for the CLG of coal. Recently, Zhang et al. [33] reported that $CaFe_2O_4$ and $Ca_2Fe_2O_5$ performed fast reaction rate, large lattice oxygen carrying capacity, high CO selectivity, and good regeneration in the coal-derived CLG process.

It is seen that calcium ferrites have exhibited a high potential to be used as OC in the CLG of coal. The above studies mainly focused on the macroscopic performance of calcium ferrites, less getting involved in the detailed analysis on the functionality of OC during the coal-derived CLG process. With respect to the promoting effects of OC on char gasification, on one side active lattice oxygen provided by the OC will help to improve the char gasification rate; on the other side, the OC could act as catalyst to accelerate the char gasification. It is necessary to identify the two positive effects of OC on char gasification, especially when considering OC may undergo complex crystal phase changes and chemical valence changes during the CLG process. In addition, the OC (including its reduced phases) may catalyze the WGS reaction, and the iron-containing substance with low oxygen potential (*e.g.*, the reduced iron oxide and calcium ferrites) will be partially regenerated with steam to produce hydrogen (typically the steam-iron reaction). The two kinds of reactions are both tightly associated with gasification products distribution, that is to say, the OC may also be effective in regulating the quality of CLG gaseous products, which certainly deserves further investigation.

In this paper, the mixed CaO/Fe_2O_3 OCs with different molar ratios of CaO to Fe_2O_3 (0:1, 0.2:0.8, 0.5:0.5, and 0.7:0.3) are prepared and investigated systematically in terms of the CLG of coal/char. The CLG performance with these CaO/Fe_2O_3 OCs is studied in a batch fluidized-bed reactor using Shengli (SL) lignite coal (char) as the fuel. The gas compositions, (instantaneous) rate of carbon conversion, and oxygen loss rate are all obtained detailedly. The contribution of lattice oxygen and catalytic substance in OCs for accelerating char gasification is carefully analyzed and the effective catalytic component is determined. In order to further understand the regulating effect of CaO/Fe_2O_3 on the CLG products, the WGS and steam-iron reactions with the addition of the re-OC particles are conducted Furthermore, the porosity and specific surface area, crystalline phase and microstructure of fresh and used bimetallic OCs are characterized by the Brunauer-Emmett-Teller (BET) analysis (Micromeritics, ASAP-2020), X-ray diffraction (XRD, X'Pert PRO) and the energy dispersive X-ray spectroscopy (EDX) coupled by environmental scanning electron microscope (ESEM, FEI Quanta 200) to better evaluate the reactivity and functionality of the OCs, as well as their resistance to agglomeration/sintering.

2. Material and methods

2.1. Material

Various CaO/Fe_2O_3 OCs are prepared as designed molar ratios of CaO to Fe_2O_3 by the wet-impregnation method. Calculated amount of $Ca(NO_3)_2{\cdot}4H_2O$ (purity > 98.5 wt%, Sinopharm, AR level) is first dissolved in deionized water, then Fe_2O_3 powder (particle size 1–75 μm, Sinopharm, AR level) is dumped into the calcium solution along with suitable citric acid (the complexing and burning agent). The mixed solution is stirred continuously by a magnetic stirring apparatus within a 90 °C water bath until the precursor is dewatered to be gelatinous. Subsequently the impregnated samples as well as the pure Fe_2O_3 are dried in a vacuum drying oven at 90 °C for 12 h and at 120 °C for another 12 h, and then calcined in a temperature-programmed muffle furnace from ambient temperature to 950 °C at 5 K/min then proceeding to keep for 5 h. As cooled down to room temperature, the calcined samples are crushed then screened to the desired size range of 180–300 μm. The received OCs with four different molar ratios of CaO to Fe_2O_3 (0:1, 0.2:0.8, 0.5:0.5 and 0.7:0.3) are denoted as FeCa0, FeCa20, FeCa50 and FeCa70, respectively.

The crystalline phase compositions of the fresh OCs are analyzed by XRD, as shown in Fig. 1. It is clear to see that the fresh FeCa0 OC is single-phase sample without impurities, only Fe_2O_3 contained. For FeCa20, Fe_2O_3 is main component, but a small amount of $CaFe_2O_4$ is also formed. As the molar ratio of CaO to Fe_2O_3 being 0.5:0.5, $CaFe_2O_4$ becomes dominant. As the CaO loading further increases (for FeCa70), the main phase in the sample changes into $Ca_2Fe_2O_5$. Besides that some remaining CaO not being combined is also found in the FeCa70 sample. From above XRD analysis, only $CaFe_2O_4$ and $Ca_2Fe_2O_5$ are formed by the combination of CaO and Fe_2O_3. The crystallite sizes of $CaFe_2O_4$ and $Ca_2Fe_2O_5$ (evaluated by Scherrer equation from the width at half-height of the more intense and better deconvoluted ray of each phase) are 45.3 nm and 31.8 nm, respectively. Note that the $Ca_2Fe_2O_5$ crystallite have a smaller size than that obtained by Zamboni et al. [34] using the same method, which indicates a better dispersion in this study.

The raw coal used as fuel is SL lignite from China. After crushed and dried at 105 °C in a vacuum drying oven, the particles of 0.3–0.5 mm

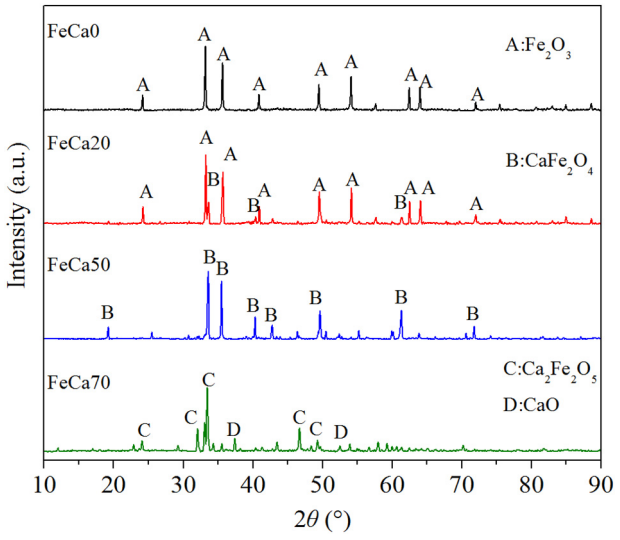

Fig. 1. XRD patterns of four fresh CaO/Fe_2O_3 samples. (A: Fe_2O_3, B: $CaFe_2O_4$, C: $Ca_2Fe_2O_5$, and D: CaO).

Table 1
Proximate and ultimate analyses of SL coal/char.

Solid fuel	Proximate analysis (wt%, ar)				Ultimate analysis (wt%, daf)				
	Moisture	Volatiles	Ash	Fixed carbon	C	H	N	S	O[a]
Coal	4.36	45.96	11.61	38.07	57.79	4.14	0.85	1.57	19.86
Coal char	1.12	7.83	19.94	71.11	72.48	0.81	0.54	3.86	2.37

[a] By difference.

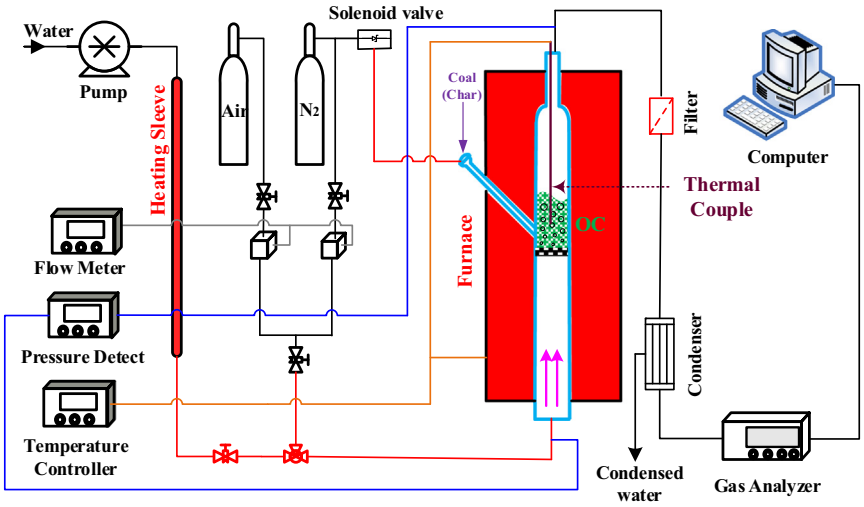

Fig. 2. Schematic layout of the batch fluidized bed reactor unit.

are collected. While the coal char is obtained by the devolatilization treatment of raw coal at 900 °C in a fixed bed within N_2 atmosphere. Proximate and ultimate analyses of the raw coal and char are presented in Table 1.

2.2. Fluidized bed setup and experimental procedure

The CLG tests with CaO/Fe_2O_3 OCs are investigated in a batch fluidized bed reactor. The schematic of the reaction system is shown in Fig. 2. The system mainly consists of a gas supplying unit, a fluidized-bed reactor, flue gas clean-up unit and a gas analysis unit. The quartz tube reactor with 26 mm inner diameter and 950 mm height is heated by an electrical furnace. And the K type thermocouple is equipped to monitor the real-time reaction temperature. A micro-porous distribution plate is located at 470 mm away from the bottom of the reactor. A feeding tube, 8 mm inner diameter and 350 mm length, is extended from a height of 10 mm above the distribution plate at a 45° direction, from which the coal (char) is introduced into the reactor with the help of high pressure N_2.

As for a typical CLG test, the OC is first added into the reactor and then the heating program is triggered. N_2 serves as the fluidization gas at a flow rate of 1200 ml/min to prevent particle agglomeration during the heating process. When the reactor temperature reaches the set point, the fluidization gas is switched to 30 vol% steam balanced by N_2 at a total flow rate of 1200 ml/min. Once the reaction atmosphere is stabilized, the solid fuel is quickly introduced into the reactor through passing high pressure N_2 from pulse solenoid valve. This operation only lasts for a few seconds, then the pulse solenoid valve is quickly closed in case of interfering the reaction zone flow state. The flue gas from the reactor passes through a high-temperature filter to remove fine particles, an electric cooler to eliminate water vapor, then is introduced into an online gas analyzer (Gasboard Analyzer 3100) to continuously detect the gas compositions of CO, CO_2, CH_4 and H_2. In the oxidation process, the fluidization gas is switched to air and the re-OC is regenerated to be ready for next test. To be noted, N_2 is used as purging gas for 5 min between oxidation and reduction.

2.3. CLG tests of coal (char) with various CaO/Fe_2O_3 OCs

All of CLG tests of coal or char are performed in the batch fludized bed reactor. The bed temperature is stabilized at 900 °C. 30 vol% steam balanced by N_2 as gasification agent is introduced from the bottom of the reactor. Each test has been repeated 3 times for accuracy concern.

The CLG test of raw coal is to gain a general knowledge of coal gasification in the presence of various CaO/Fe_2O_3 OCs. To maintain similar fludization environment, here the weight ratio of each OC to coal is set as 15 g: 0.65 g. The carbon conversion, low heating value of the gas products, and gas distribution are assessed. The CLG test of coal char is to gain insight into the reactivity and functionality of the CaO/Fe_2O_3 OCs. The real-time gas compositions, carbon conversion rate as well as oxygen loss rate are analyzed. Differently, the mass ratio of OC to char is changed into 15 g: 0.38 g. Furthermore, considering the promoting effects of the partially reduced OCs on the char gasification, the re-OCs are utilized again for the same char CLG experiment. This series of char gasificartion test is to identify that the OC contribution to char gasification is from lattice oxygen or catalyst.

The standard deviation of each gas composition is < 5%. For raw coal, the maximum standard deviation is 3.45% for CO_2 when FeCa0 is used as oxygen carrier (OC). For coal char, the maximum standard deviation is 3.78% for H_2 when FeCa70 is used as OC. The relatively small standard deviation can ensure the repeatability and reliability of the collected data.

2.4. Experiments of the WGS and steam-iron reactions

The WGS experiments with four partially reduced samples (each with 1 g) from the char gasification tests are performed in a fixed bed with the temperature range of 600–950 °C. These experiments are

designed for exploring the catalytic effect of partially re-OCs on the WGS reaction. In each test, 10 vol% CO balanced by N_2 at a total flow rate of 300 ml/ min, together with steam of 124 ml/min, is employed as reactive gas. And the flue gas concentration is monitored by the gas analyzer in real-time until it keeps relatively steady concentration (with a fluctuation range of ± 5%) for 5 min.

The deep reduction of these OCs during the CLG process may occur, where FeO or even Fe phase may be generated. They are easy to be oxided by steam to produce hydrogen (typically the steam-iron reaction), which affects the distribution and quality of the gas products in the coal gasification process. Thus, it is necessary to conduct individual experiments to study the steam-iron reaction based on different OCs after deep reduction. These fresh OCs are reduced by simulated synthesis gas, which contains 20 vol% CO, 10 vol% H_2, 10 vol% CO_2 and 5 vol% CH_4, balanced by N_2. The steam-iron tests with the presence of four deeply reduced OCs (dre-OCs, initially 5 g Fe_2O_3 contained in all fresh samples) are carried out in the batch fluidized bed reactor at 900 °C, and the steam concentration in each test is always maintained at 30 vol% (balanced by N_2 at a flow rate of 840 ml/min). Meanwhile, the real-time H_2 concentration is monitored for subsequent evaluation. Additionally, to recover fully oxided state of these dre-OCs for cyclic test, after steam oxidation they are re-oxided by air at a flow rate of 840 ml/min.

2.5. Characterization of CaO/Fe_2O_3 OCs

The XRD (X'Pert PRO) is used to identify the crystalline phases on a Empyrean X-ray diffraction meter with Cu Kα radiation (k = 1.5418 Å) in the 2θ range of 10–90° with a rate of 5° min^{-1} at 30 kV and 30 mA. And the morphological and structural changes of the OCs are analyzed by the ESEM with the accelerating voltage of 20.0 kV. The magnification level of 2500× is chosen for both fresh and used OCs. Moreover, the EDX coupled by ESEM is employed to investigate the elemental distribution on the surface of OC particles. In addition, the surface area and pore characteristics of the samples were measured by the BET method. The crushing strength of the OCs is measured by a digital dynamometer (Shimpo FGJ-5). For accuracy concern, each strength measurement is repeated for 5 times.

2.6. Date evaluation

The data evaluation methods adopted in this work are presented in Table 2.

$\boldsymbol{t}$: reaction time; $\boldsymbol{q_f}$: the gas volumetric flow rate at the outlet of the reactor under standard conditions; $\boldsymbol{y_i}$: the molar fraction of each component i in outlet stream; $\boldsymbol{i}$: H_2, CO, CO_2 and CH_4, respectively; $\boldsymbol{M_{total}}$: the mass of solid fuel in each test; $\boldsymbol{V_i}$ is the total volume fraction of gas i in the total gas; $\boldsymbol{m_C(t)}$: the total amount of carbon converted into gas phase during time t; $\boldsymbol{m_{total}}$: the total amount of carbon in the fuel; $\boldsymbol{q_f'}$: the volumetric flow rate of feeding gas in the fixed bed; $\boldsymbol{y_{CO}'}$: the molar fraction of CO in the feeding gas.

3. Results and discussion

3.1. The CLG of coal with various CaO/Fe_2O_3 OCs

For a coal-derived CLG process, the main reactions involved are as follows:

$$\text{Coal} + \text{heat} \rightarrow \text{Char} + \text{volatile (CO, } H_2\text{, } CO_2\text{, } CH_4\text{, } C_nH_m) \quad \text{(R1)}$$
$$C + H_2O \rightarrow CO + H_2 \quad \Delta H_{900^\circ C} = 135.71 \text{ kJ/mol} \quad \text{(R2)}$$
$$C + CO_2 \rightarrow 2CO \quad \Delta H_{900^\circ C} = 168.84 \text{ kJ/mol} \quad \text{(R3)}$$
$$CO + H_2O \rightarrow CO_2 + H_2 \quad \Delta H_{900^\circ C} = -33.13 \text{ kJ/mol} \quad \text{(R4)}$$
$$CH_4 + H_2O \rightarrow CO + 3H_2 \quad \Delta H_{900^\circ C} = 225.70 \text{ kJ/mol} \quad \text{(R5)}$$
$$CH_4 + OC(\text{oxidation}) \rightarrow CO(CO_2) + H_2(H_2O) + OC(\text{reduction}) \quad \text{(R6)}$$
$$CO(H_2) + OC(\text{oxidation}) \rightarrow CO_2(H_2O) + OC(\text{reduction}) \quad \text{(R7)}$$

Table 2
The summary of evaluation formulas.

Items	Formulas	Number
Gas volume fraction, %	$Y_i = \frac{\int_0^t q_f y_i dt}{\int_0^t q_f (y_{CO} + y_{CO_2} + y_{H_2} + y_{CH_4}) dt}$	(1)
Syngas yield, Nm^3/kg	$G_{syn} = \frac{\int_0^t q_f (y_{CO} + y_{CH_4} + y_{H_2}) dt}{M_{total}}$	(2)
Ratio of H_2/CO	Y_{H_2}/Y_{CO}	(3)
Low heating value (LHV) of gas products, MJ/Nm^3	$12.64 \times V_{CO} + 35.88 \times V_{CH_4} + 10.79 \times V_{H_2}$	(4)
Carbon conversion, %	$X_C = \frac{m_C(t)}{m_{total}}$	(5)
Carbon conversion rate, s^{-1}	dX_C/dt	(6)
Instantaneous rate of carbon conversion, s^{-1}	$r_C = \frac{dX_C/dt}{1 - X_C}$	(7)
Oxygen loss rate from OC [26], g/s	$r_{oxygen} = \frac{16 q_f (2y_{CO_2} + y_{CO} - y_{H_2})}{22.4}$	(8)
CO conversion for the WGS reaction, %	$X_{CO} = \frac{q_f' y_{CO}' - q_f y_{CO}}{q_f' y_{CO}'} \times 100\%$	(9)
Selectivity for the WGS reaction	$S_{CO} = \frac{q_f y_{CO_2}}{q_f' y_{CO}' - q_f y_{CO}}$	(10)
H_2 yield for the steam-iron reaction, ml	$\int_0^t q_f y_{H_2} dt$	(11)
H_2 production rate for the steam-iron reaction, ml/s	$q_f y_{H_2}$	(12)

Among these reactions, R2 and R3 are the basic steps to gasify solid carbon into carbonaceous gases, while R4 to R7 are tightly associated with the ultimate distribution of the gas products. The carbon conversion and gas LHV are shown in Table 3. There shows an obvious gas LHV upward trend with the increase of CaO addition. And the highest carbon conversion of 90.67% is achieved when using FeCa0 as OC, which is slightly higher than that of FeCa50. However, the gas LHV of 6.29 MJ/Nm^3 in FeCa0 is significantly lower than 9.17 MJ/Nm^3 in FeCa50. Actually, the addition of CaO implies a decrease in the proportion of active lattice oxygen carried by per unit weight of OC, which means the syngas concentration will be potentially higher and CO_2 concentration will be lower in the gas products with the increase of CaO addition. This can also be validated by gas distribution shown in Fig. 3. The combustible gases consist mainly of CO and H_2, and less CH_4 is also observed. As known, CO and H_2 have the potential to exihibit a gasification inhibitation for R2 and R3 [35]. This can be the main reason why lower carbon conversions are attained in the cases of FeCa20 and FeCa70. Nevertheless, the carbon conversion in FeCa50 does not present an obvious decline compared to FeCa0, which may be attributed to the action of catalytic substance in FeCa50.

Fig. 3 compares the gas compositions during the coal-derived CLG process with different OCs. As seen, the H_2 concentration is always maintained at the highest level, except in the FeCa0 case where more active lattice oxygen available combusts pyrolysis/gasification products to generate the highest CO_2 concentration. It is no wonder that the H_2 concentration presents an overall upward trend with the decrease of active content in the OC, and the trend is just opposite for CO_2. Obviously, a higher active content per unit weight of OC means a larger amount of syngas consumption during the CLG process. Meanwhile, an obvious rise of CO concentration in FeCa70 also reveals an insufficient lattice oxygen supply. In all tests, the CH_4 concentration does not change a lot.

To exhibit a more accurate evaluation on the gas production generated at various OCs, the gas yield and H_2/CO ratio are plotted in Fig. 4. As seen, the decreasing Fe_2O_3 content in OCs is favorable for an increase of syngas yield, nevertheless, the increase is mainly due to more H_2 generated when OCs used changes from FeCa0 to FeCa50. Additionally, the H_2/CO ratio does not present a regular change. As for

Table 3
Effect of OCs on carbon conversion and gas LHV with SL coal.

OC	FeCa0	FeCa20	FeCa50	FeCa70
Carbon conversion (%)	90.67 ± 1.23	83.87 ± 0.97	89.73 ± 1.55	86.67 ± 1.08
Gas LHV (MJ/Nm^3)	6.29 ± 0.14	6.75 ± 0.14	8.01 ± 0.19	9.17 ± 0.10

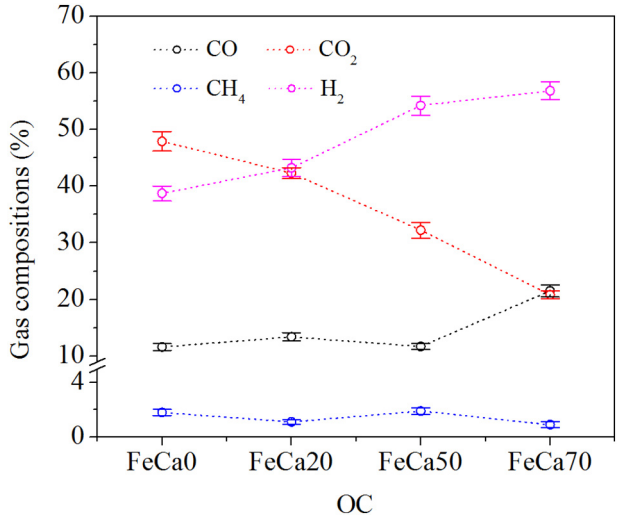

Fig. 3. Effect of OCs on total gas compositions with SL coal. (Mass of OC: 15 g; coal: 0.65 g; temperature: 900 °C; steam concentration: 30 vol%.)

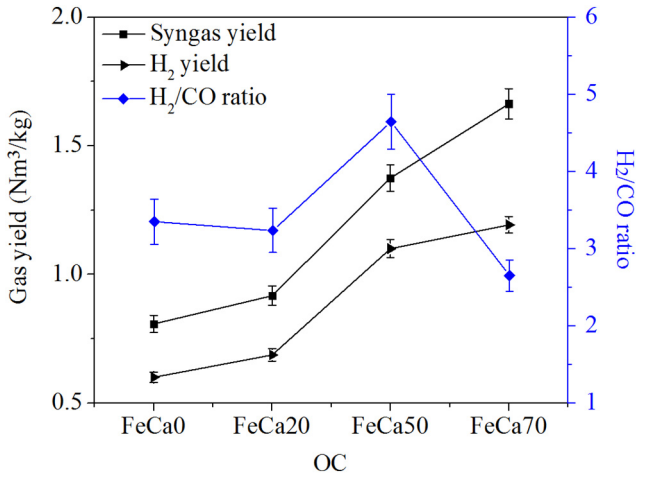

Fig. 4. The gas yield and H_2/CO ratio at different OCs with SL coal. (Mass of OC: 15 g; coal: 0.65 g; temperature: 900 °C; steam concentration: 30 vol%.)

FeCa50, the syngas yield is 1.4 Nm^3/kg and its H_2/CO ratio attains the maximum value of 4.6. Although FeCa70 exhibits the highest syngas yield of 1.7 Nm^3/kg, the H_2/CO ratio of 2.7 is relatively lower, which is unfavorable to obtain rich hydrogen product. However, we should note here that a smaller active content in OC will increase the OC inventory per unit thermal power of coal during the CLG process. In this sense, a balance between gas quality and active content in OC should be evaluated comprehensively when turning to industrial application.

3.2. The promoting effect of CaO/Fe_2O_3 OCs on the char gasification

3.2.1. Gas distribution and evolution during the CLG of char with various CaO/Fe_2O_3 OCs

Fig. 5 shows the gas compositions and oxygen loss rate *versus* time based on various OCs during the char gasification process. As seen from the distribution of gas concentration, entire process can be roughly divided into two stages: the first stage is a rapid rising process for each gas component, which can reach respective peak value in a short time. Higher CO_2 concentration lasting for a longer time means that there coexists stronger combustion reaction (R7). From this perspective, the combustion process is gradually weakened with the decrease of active lattice oxygen content in OCs. Note that a highest CO_2 concentration peak is presented in FeCa50, which is mainly attributed to its excellent lattice oxygen release characteristics compared to other three OCs, while the sharp pattern of CO_2 peak means a shorter duration mainly due to relative lower active content in FeCa50. On the other side, the second stage presents a slow decreasing process, where each gas component declines slowly and the duration is longer.

For FeCa0, the CO_2 concentration exhibits a peak value of 5.4% at 180 s, which is close to the time when the maximum oxygen loss rate is achieved. Moreover, this peak is significantly higher than that of CO (1.5%) and H_2 (2%) near 100 s, and this phenomenon results from rich lattice oxygen comsuming more CO and H_2 to form CO_2 and H_2O. While for FeCa20, the CO_2 concentration reaches its peak value of 3.9% at 100 s, which is lower than that in FeCa0. It can be attributed to the decreasing oxygen loss rate due to the declining active content in FeCa20, which can be reflected straightfowardly from the total oxygen loss percentage (total oxygen loss amount/theoretical oxygen loss amount from Fe_2O_3 to Fe_3O_4) as well as the maximum oxygen loss rate. As listed in Table 4, the total oxygen loss percentage and the maximum oxygen loss rate drop from 76.0% and 1.1×10^{-3} in FeCa0 to 47.9% and 7.0×10^{-4} g/s in FeCa20, respectively. During this process, the H_2 concentration maintains the highest relative to CO_2 and CO. For FeCa50, it exhibits a shorter oxygen loss time due to the relatively lower active content contained. Nevertheless, it is interesting to find that its oxygen loss rate receives the maximum value of 1.2×10^{-3} g/s at 80 s compared to other three OCs and the total oxygen loss percentage is 70.2%, only slightly lower than that of FeCa0. It indicates the $CaFe_2O_4$ phase in FeCa50 possesses a better oxygen transfer characteristics. In addition, the oxygen loss rate in FeCa70 exhibits a fluctuation around 0. It can be attributed to the good thermodynamic stability of $Ca_2Fe_2O_5$ (the main active phase in FeCa70). To be noted, a negative oxygen loss rate is found in FeCa70, which implies that a small amount of reduced phase is oxidized by steam, presenting an oxygen acquisition in the oxygen loss curve. To facilitate the comparison, the detailed data about oxygen loss are listed in Table 4.

To evaluate the char gasification performance with these OCs, the gas distribution, gas yield and H_2/CO during the CLG of coal char are shown in Fig. 6 and Fig. 7. The results suggest that rich active content favors fuel gas combustion, explaining why the lowest and highest syngas yields are obtained in FeCa0 and FeCa70, respectively. Similar to the coal-derived CLG process, the evolution of H_2 yield follows basically that of the syngas yield. Furthermore, similar gas compositions between FeCa20 and FeCa50 can be attributed to approximative total oxygen loss amount, as counted in Table 4. For FeCa50, the highest H_2/CO ratio is achieved, which is consistent with the results when using coal as fuel, further demonstrating that the FeCa50 possesses a potential ability to obtain rich hydrogen production.

3.2.2. The effect of various CaO/Fe_2O_3 OCs (and their partially reduced samples) on the char gasification rate

The (instantaneous) rate of carbon conversion of four OCs with coal char are shown in Fig. 8. Both FeCa0 and FeCa50 can achieve higher

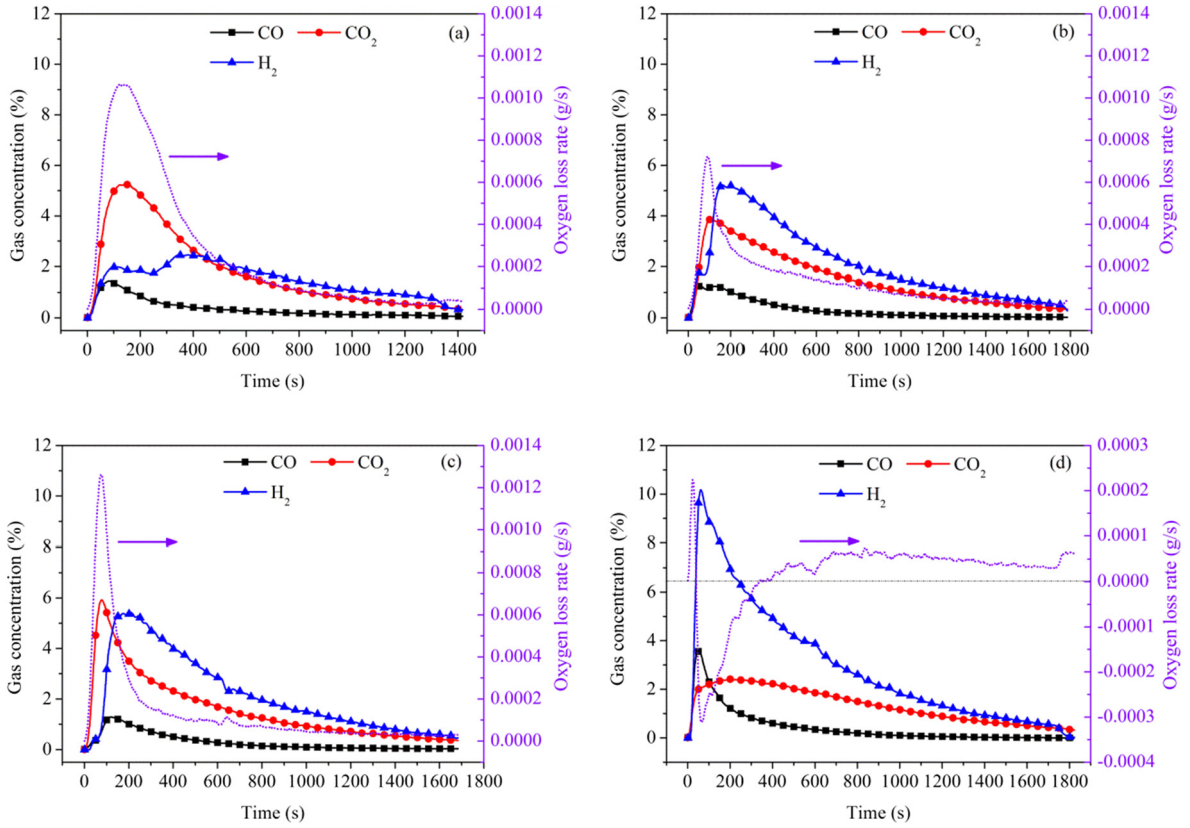

Fig. 5. Gas concentration and oxygen loss rate profiles at (a) FeCa0, (b) FeCa20, (c) FeCa50, and (d) FeCa70 with SL coal char. (Mass of OC: 15 g; char: 0.38 g; temperature: 900 °C; steam concentration: 30 vol%.)

Table 4
The oxygen loss at various CaO/Fe_2O_3 OCs with SL coal char.

OCs	FeCa0	FeCa20	FeCa50	FeCa70
Maximum oxygen loss rate (g/s)	1.1×10^{-3}	7.0×10^{-4}	1.2×10^{-3}	2.3×10^{-4}
Time (s)	160	100	80	20
Total oxygen loss amount (g)	0.38	0.22	0.26	0.03
Total oxygen loss percentage (%)	76.0	47.9	70.2	10.9

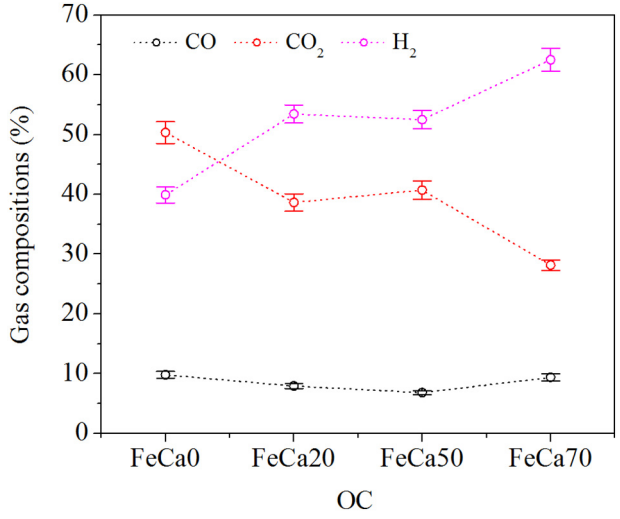

Fig. 6. Effect of OCs on gas compositions with SL coal char. (Mass of OC: 15 g; char: 0.38 g; temperature: 900 °C, steam concentration: 30 vol%.)

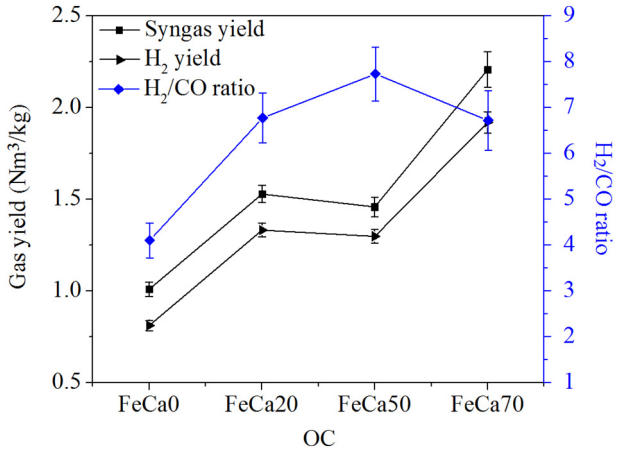

Fig. 7. The gas yield and H_2/CO ratio at different OCs with SL coal char. (Mass of OC: 15 g; char: 0.38 g; temperature: 900 °C, steam concentration: 30 vol%.)

carbon conversion rate peaks compared to FeCa20 and FeCa70. Additionally, the instantaneous carbon conversion rates with these four OCs are presented in Fig. 8(b). In particular, to avoid any possible effect of the back-mixing at the beginning or mathematical errors introduced at the end of the period when the concentrations or remaining char are too low [36], only the instantaneous rate of carbon conversion at steady state ($0.1 < X_C < 0.85$) is considered as a representative of the process. As observed from the steady pattern, FeCa0 and FeCa50 perform better promoting effect on char gasification than FeCa20 and FeCa70. As X_C is lower than 0.37, the instantaneous carbon conversion rate in FeCa0 is higher than that in FeCa50, which can be attributed to that rich lattice oxygen weakens the coal char gasification inhibition from CO and H_2. However, When $X_C > 0.37$, the instantaneous carbon

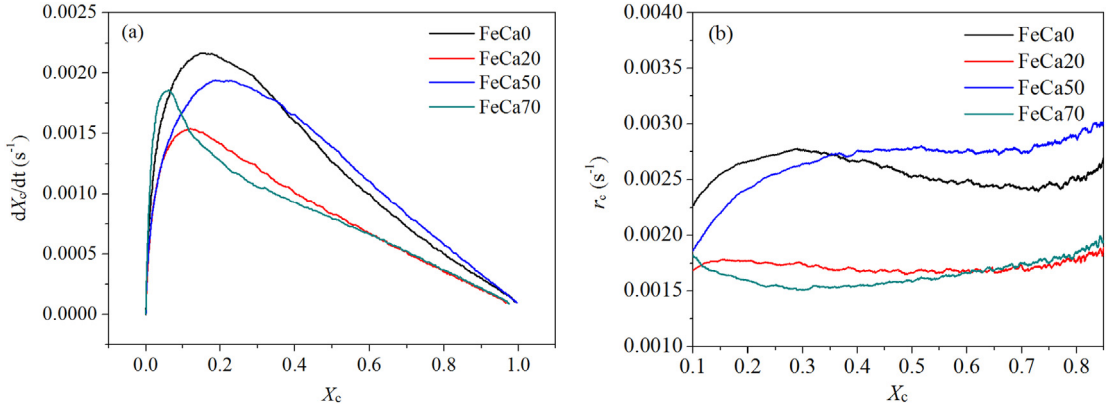

Fig. 8. The rate of carbon conversion (a) and instantaneous rate of carbon conversion (b) at various OCs with SL coal char. (Mass of OC: 15 g; char: 0.38 g; temperature: 900 °C, steam concentration: 30 vol%.)

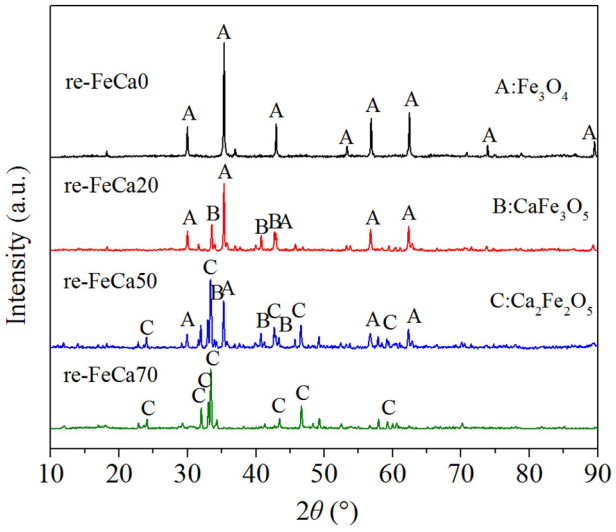

Fig. 9. XRD patterns of various re-OCs from coal char test in fluidized bed reactor.

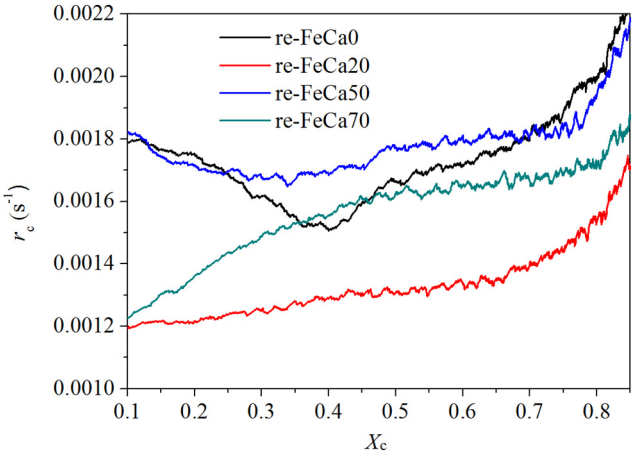

Fig. 10. The instantaneous rate of carbon conversion at various re-OCs with coal char. (Mass of char: 0.38 g; temperature: 900 °C, steam concentration: 30 vol%.)

conversion rate in FeCa50 was in turn higher than that in FeCa0, which can be ascribed to the effect of catalytic substance. To be noted, FeCa20 also performs the lowest carbon conversion, which can be explained by moderate oxygen loss rate (see Table 4) and the absence of catalytic substance (see Fig. 9). By comparison with the results of coal as fuel, it is noted that FeCa50 always behaves better conversion characteristics regardless of coal or char.

Fig. 9 shows the XRD patterns of the re-OCs, which are derived from above coal char CLG test. As seen, Fe_3O_4 is the common phase detected in the re-FeCa0, re-FeCa20 and re-FeCa50. Differently, minor Fe_3O_4 phase in the reduced Ca-containing samples is derived from the reduction of $CaFe_2O_4$, which can be deduced from the crystal phase change in the FeCa50 between fresh and reduced. In addition, $Ca_2Fe_2O_5$ is also detected in the re-FeCa50, and it is still the major phase in re-FeCa70 and remains unchanged.

To further identify the catalytic substance, the re-OCs are then utilized for the same char CLG experiment. The instantaneous carbon conversion rate of various re-OCs are shown in Fig. 10. During this process, the lattice oxygen contribution to char gasification is remarkably weakened, conversely, the catalytic effect is highlighted. And this may be the main reason why the instantaneous rate of carbon conversion in re-FeCa70 is obviously higher than that in re-FeCa20, which is opposite to the case presented in Fig. 8(b). Therefore we deduce that $Ca_2Fe_2O_5$, the major phase in the re-FeCa70, is exactly the catalytic substance on the char gasification.

Combining Fig. 8 and Fig. 10, we deduce that the char gasification rate depend on both lattice oxygen donation ability and catalytic activity of OCs. For all CaO/Fe_2O_3 OCs, the early contribution relies more on active lattice oxygen donation, while the catalysis is prominent at the later stage of char gasification when the OCs' lattice oxygen denotion ability reduces and/or the catalytic substances emerge.

3.3. The regulating effect of various CaO/Fe_2O_3 OCs on the coal gasification products

3.3.1. The catalytic effect of partially re-OCs on the WGS reaction

The WGS reaction (R4), being reversible and exothermic moderately, is an important step for the regulation of gas products during the CLG process. In view of the fact that H_2O activation is a rate-limiting step for the WGS reaction, different bimetallic catalysts [37–40] had already been investigated to improve the CO equilibrium conversion and the selectivity. Some common characteristics of WGS catalysts are available oxygen vacancies, activity for the dissociation of water [41]. Fe_3O_4 was reported to be the active phase for WGS catalysis, which is initially presented as Fe_2O_3 before the fuel gas reduction [42]. Boreskov et al. [43,44] had demonstrated that magnetite-based catalysts can be highly effective for the complete dissociation of H_2O into H_2 and adsorb oxygen under high temperature WGS reaction condition. Thermodynamically, high temperature is not conducive to forward reaction but indeed causes high reaction rate. The exploring temperature of 600–950 °C is selected based on a practical CLG process.

The equilibrium CO conversion is calculated by [45]

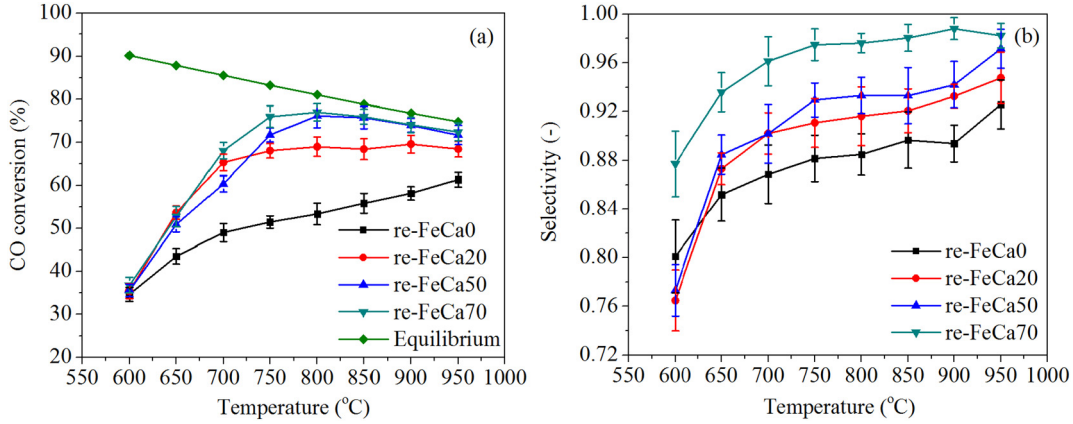

Fig. 11. The CO conversion (a) and selectivity (b) in the WGS process at various re-OCs. (Mass of reduced OCs: 1 g; reactive gas: 10 vol% CO balanced by N_2 at a total flow rate of 300 ml/min, together with steam of 124 ml/min.)

$$k_{eq} = \frac{X_{CO}^2}{(1 - X_{CO})(\lambda - X_{CO})} = \exp[A(A(0.63508 - 0.29353A) + 4.1778) + 0.31688] \quad (13)$$

$$A = 1000/T - 1 \quad (14)$$

where X_{CO} is the CO conversion under thermodynamic equilibrium state; λ is the molar ratio of H_2O to CO; A and T are the parameter and thermodynamic temperature, respectively.

Fig. 11(a) shows the variation of CO conversion in the presence of different re-OCs. As seen, the CO conversion presents elevated trend with the increase of reaction temperature from 600 to 800 °C, which may be attributed to the activation of OCs' catalytic ability beyond the effect of thermodynamic limitation. And this is favorable for approaching to the theoretical thermodynamic equilibrium. However, the CO conversion presents slight decline from 800 to 950 °C in the re-FeCa50 and re-FeCa70, which may result from further enhancement of the thermodynamic limitation. Note that, increasing CaO content also leads to the elevation of CO conversion. On the one hand, the incorporation of CaO can form more oxygen vacancies, which in turn enhances the oxygen mobility in catalysts [46]. On the other hand, CaO addition likely improves the adsorption strength of CO molecules as well as inhibits excess water molecules from covering active sites effectively, which is possibly similar to the role of Cu dopants in the Fe_3O_4 surface [47]. The CO conversion attains the highest value of 77% in the re-FeCa70 at 800 °C among four samples. Keeping the chemical components of various partially re-OCs (identified in Fig. 9) in mind, we deduce that both $Ca_2Fe_2O_5$ and $CaFe_3O_5$ own a better catalytic activity than Fe_3O_4, while these two Ca—Fe phases have similar activities between 600 and 700 °C by comparing the CO conversion at Ca-containing samples in Fig. 11(a). Moreover, there shows the higher CO conversion in re-FeCa50 and re-FeCa70 than that in re-FeCa20 above 700 °C, which proves the stronger catalytic activity of $Ca_2Fe_2O_5$ than $CaFe_3O_5$ (see the XRD analysis for the substance identification). In addition, both the CO conversions in the re-FeCa50 and re-FeCa70 are quite close to the thetheoretical value above 800 °C, which is conducive to guiding the H_2/CO regulation based on the thermodynamic calculation.

Except for the catalytic activity, the selectivity is another vital index of a catalyst. In addition to the H_2 and CO_2 production, CO may be partially converted into CH_4, methanol or other organic compounds. Tanaka and Iizuka [48] reported that the formation of CH_4 appeared to occur through the WGS reaction over supported rhodium catalysts, followed by the hydrogenation of carbonaceous species formed by the dissociation of CO or CO_2. Additionally, Il'in et al. [49] found that methyl acetate and methanol were the most abundant by-products at 330–360 °C when calcium ferrite used as a catalyst. Therefore, the production selectivity based on four re-OCs is also investigated, as presented in Fig. 11(b). Both the increase of CaO content and temperature can improve the selectivity to R4, which presents similar regularity in terms of the CO conversion. And the selectivity increases from 0.85 to 0.93 in re-FeCa0 and 0.94 to 0.98 in re-FeCa70 when increasing temperature from 650 to 950 °C. Similarly, by combining with the phase patterns in Fig. 9, the ultimate selectivity order of the catalytic phase is determined as $Ca_2Fe_2O_5$ (strong), $CaFe_3O_5$ (moderate) and Fe_3O_4 (weak).

3.3.2. *The dre-OCs reacting with H_2O to produce H_2*

The propensity of metallic iron or low-valent iron oxides being oxidized by steam to produce hydrogen at high temperatures is well known. Nevertheless, the unmodified FeCa0 is easy to deactivate quickly when it is reduced as deeply as the Ca-containing materials. Since the addition of CaO forming ferrites alters the equilibrium oxygen fugacity for the phase transitions [31], this section will examine the effect of CaO on the phase transitions between steam oxidation and deep reduction.

The phase distributions of these dre-OCs are presented in Fig. 12. As seen, the FeO is main low-valence iron oxide in dre-FeCa0 and dre-FeCa20, which is also the dominant hydrogen producer due to the thermodynamic limitation of steam oxidation of Fe_3O_4. Nevertheless, the Fe phase is found in dre-FeCa50 and dre-FeCa70, which has an

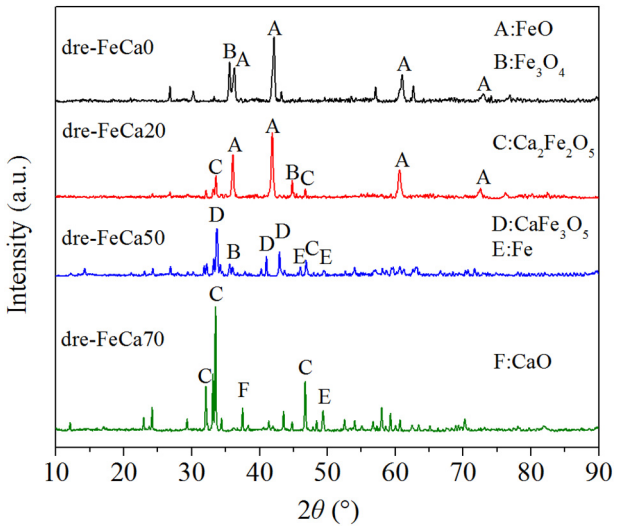

Fig. 12. XRD results of various dre-OCs from deep reduction. (Synthesis gas used for deep reduction: 20 vol% CO, 10 vol% H_2, 10 vol% CO_2 and 5 vol% CH_4, balanced by N_2).

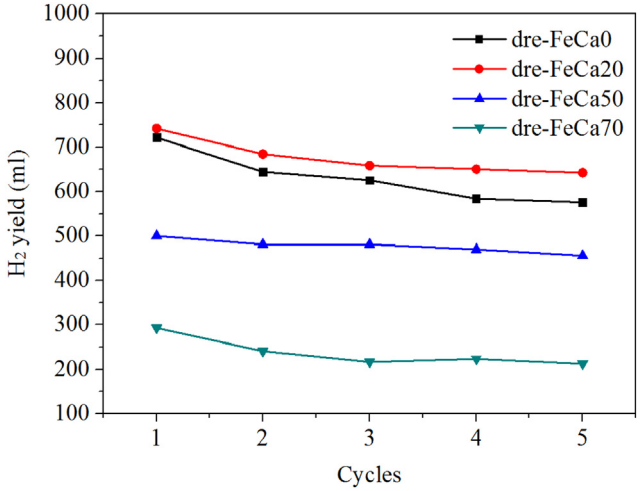

Fig. 13. The H_2 yield at various dre-OCs *vs.* cycle numbers.

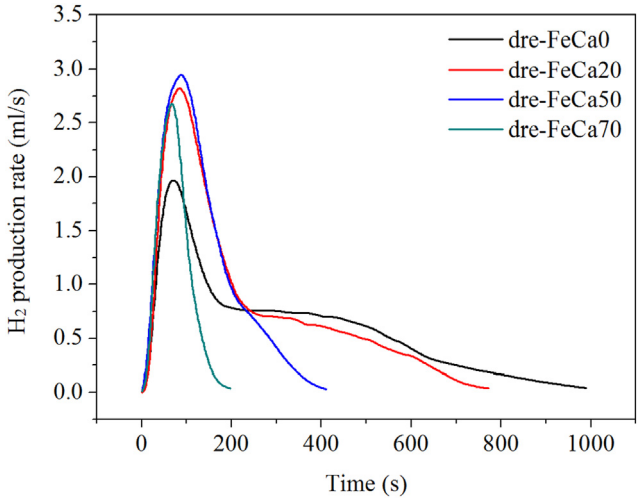

Fig. 14. The H_2 production rate at various dre-OCs in the fifth cycle.

advantage over FeO in hydrogen production.

Fig. 13 shows the H_2 yield of four dre-OCs in the cyclic test. As seen, the dre-FeCa20 always presents the highest H_2 yield in five cycles, which is opposite to the dre-FeCa70. Clearly, the H_2 yield of the dre-OC is related to the components of iron-containing substance with low oxygen potential (*e.g.*, the reduced iron oxide and calcium ferrites) as well as its oxidation characteristics. Together with Fig. 12, it can be deduced that the forming $Ca_2Fe_2O_5$, with a poor reducibility due to its low equilibrium p_{O2} thermodynamically, leads to the decrease of reducible component. And this necessarily limits the H_2 yield, which is closely dependent on the reduced phase. Additionally, the main reduced phase of FeCa50 is $CaFe_3O_5$, which generates a rather lower H_2 yield compared to the deeper reduced phase FeO in FeCa0 and FeCa20.

Fig. 14 depicts the H_2 production rate in the fifth steam oxidation operation, in the presence of different dre-OCs. Obviously, the H_2 production rate depends not only on crystalline phase and its reduction level, but also on the the kinetics of steam oxidation reaction and the diffusion process [50]. Noting that the hydrogen is mainly yielded within 200 s, and the H_2 production rate peaks in dre-FeCa20 and dre-FeCa50 are 2.82 ml/s and 2.95 ml/s, respectively, both larger than 2.67 ml/s in dre-FeCa70 and 1.96 ml/s in dre-FeCa0. Together with the XRD analysis in Fig. 12, we deduce that the significant rate difference between dre-FeCa0 and dre-FeCa20 can only result from $Ca_2Fe_2O_5$, which is able to provide active sites to enhance the adsorption strength and the numbers of adsorbed water molecules, as confirmed by the higher rate peak in dre-FeCa70 (even small amount of reduced phase available). The highest rate peak acquired in dre-FeCa50 should be attributed to both the forming reduced phase (especially Fe) and the contribution by $Ca_2Fe_2O_5$.

3.4. Characterization of CaO/Fe_2O_3 OCs

The morphological and structural changes for the fresh and used (after air oxidation, which are the ones after char CLG test) CaO/Fe_2O_3 OCs are shown in Table 5. The specific surface area of the fresh OCs increases gradually with the increase of CaO content, and that is opposite to the mechanical strength. Therefore, the addition of CaO is bad for particle strength even though some Ca—Fe phases can be formed. Nevertheless, it is still able to meet the requirements of chemical looping process in fluidized beds (> 1 N). Moreover, the pore size of all fresh OCs is similar, but the pore volume of the FeCa70 sample is almost twice as large as others, which may cause a sharp drop in particle strength. As for the used samples, both the specific surface area and pore volume decrease obviously, which may be attributed to the ash paticles deposition or the sintering of relative low-valence phase during the CLG process. Additionally, the mechanical strength of all used OCs only presents slight decrease, which is worth further investigation during a multi-cycle test.

Fig. 15 shows the ESEM-EDX images of the fresh and used CaO/Fe_2O_3 OCs. With respect to the surface morphology of the used OC particle, both the FeCa0 and FeCa20 display relatively rough as well as some surface particles aggregation. While FeCa50 and FeCa70 remain smooth structure and change little. Sintering phenomenon is not observed on the surface of both OC particles. The EDX results indicate that Fe, Ca, and O are detected in both Ca-containing samples, while Si is only detected in used FeCa20, which may come from the ash deposition during the CLG process. To be noted, the detected C is derived from the carbon coating on the particles (to enhance the electrical conductivity of the particles) before the ESEM tests. Additionally, the peak intensity ratio of Ca to Fe in the used FeCa50 is obviously higher than that in the fresh one, which can be attributed to the enrichment of Ca element during the conversion of $CaFe_2O_4$ to $Ca_2Fe_2O_5$.

Table 5
The physical characterization of the fresh and used CaO/Fe_2O_3 OCs.

OCs	Specific surface area (cm^2/g)		Pore volume (ml/g)		Pore size (nm)		Mechanical strength(N)	
	Fresh	Used	Fresh	Used	Fresh	Used	Fresh	Used
FeCa0	0.75	0.36	0.0023	0.0009	12.27	11.14	3.23 ± 0.12	3.21 ± 0.12
FeCa20	0.82	0.42	0.0024	0.0012	11.76	10.23	3.19 ± 0.13	3.18 ± 0.10
FeCa50	0.98	0.67	0.0028	0.0015	11.43	10.08	2.78 ± 0.15	2.72 ± 0.11
FeCa70	1.46	1.08	0.0047	0.0023	12.84	12.03	1.89 ± 0.11	1.86 ± 0.12

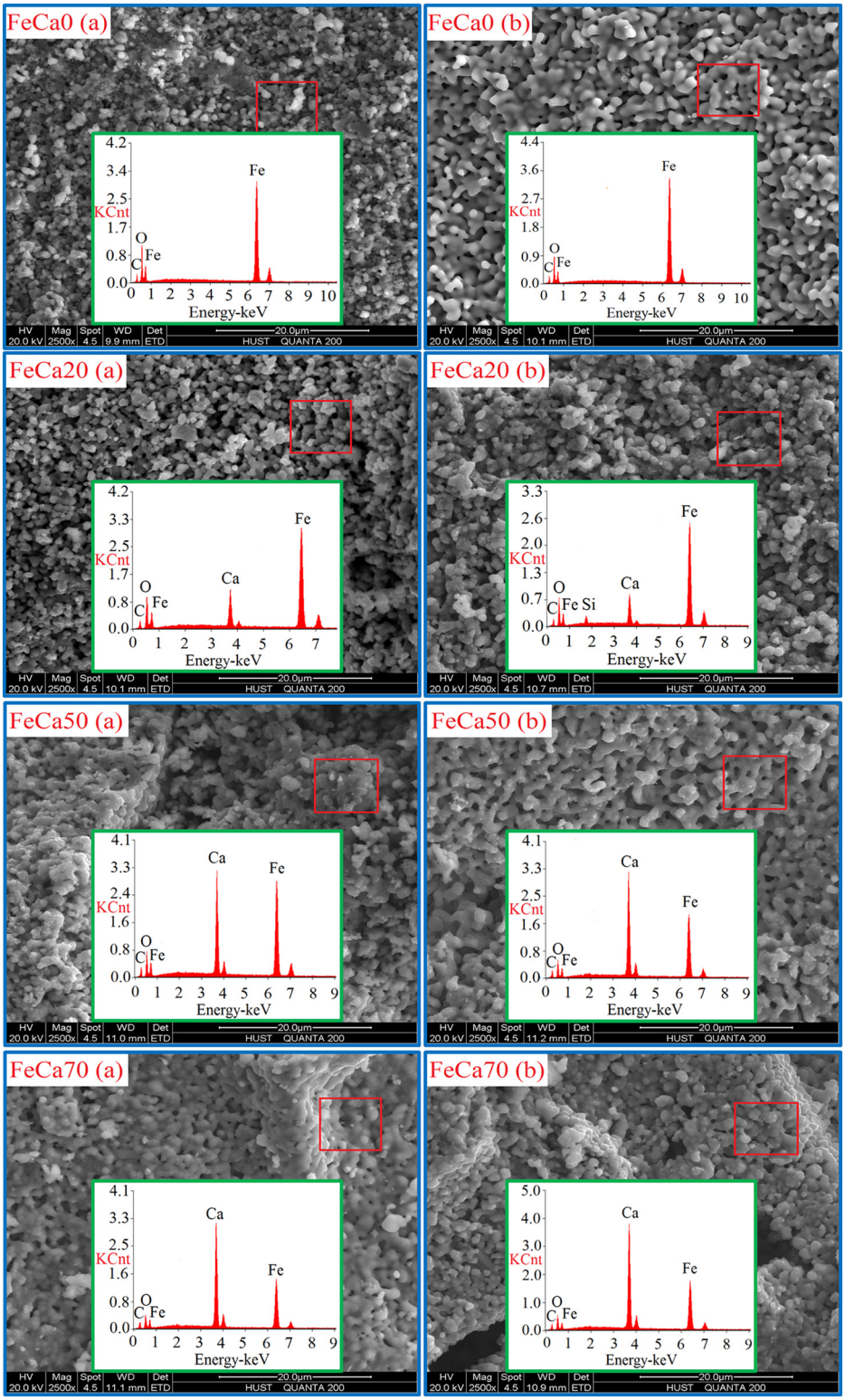

Fig. 15. ESEM images (magnification of 2500×) and EDX analyses of fresh (a) and used (b) samples (oxidation state) from char CLG tests.

3.5. Discussion

Undoubtedly, CaO/Fe_2O_3 OCs have a promoting role in the char gasification, mainly including two routes: active lattice oxygen contribution and catalytic effect. The former is tightly associated with lattice oxygen donation ability which is crucial for chemical looping process regardless of full or partial oxidation of fuel. To be close to an industrial process without enough residence time for deeper reduction, the designed gasification tests mainly consider the step of oxygen donation from Fe_2O_3 to Fe_3O_4, which is also confirmed by the total oxygen loss amount listed in Table 4 and the XRD patterns presented in Fig. 9. In the initial period, the former contribution is prominent, which is ascribed to fuel gas consumption in R7 (decreasing the gasification inhibitation and producing heat) facilitating the forward movement of

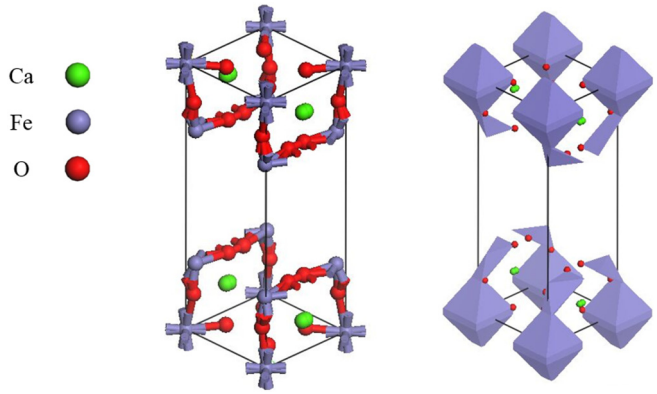

Fig. 16. Crystal structure of $Ca_2Fe_2O_5$. (Geometrically optimized and the lattice constant of unit cells adopted from reference [51].)

R2. On the other side, the catalytic effect is usually highlighted at the later stage of solid fuel reaction when the lattice oxygen donation ability of OC reduces. During this period the reduced phases play an important catalytic role in solid fuel gasification. However, the catalysis from some saturated oxides like $Ca_2Fe_2O_5$ should also be noted.

The crystal structure of $Ca_2Fe_2O_5$, which is geometrically optimized (the lattice constant of unit cells is adopted from reference [51]) based on the Gibbs free energy minimization, is depicted in Fig. 16. Iron atom is coordinated with oxygen atom to form two polygonal structures of octahedron and tetrahedron (FeO^{-6} and FeO^{-4}), and the structure contains alternating parallel iron-oxygen octahedra and tetrahedra with calcium atoms in holes between the polyhedra of nine oxygen atoms [52]. The oxygen vacancies forming from the slight shift of the iron atoms from the cubic perovskite structure will contribute to the mobility of oxygen [53,54], which is favorable for the oxygen ions dissociation from water by active sites, then further combining with CO to form CO_2 [34]. Generally, the presence of $Ca_2Fe_2O_5$ is beneficial to the forward contribution of the WGS reaction, together with a better selectivity for R4. The catalytic properties of $Ca_2Fe_2O_5$ have been reported in some literatures [49,55,56], but mainly focusing on the gas fuel conversion at below 500 °C and less getting involved in the solid fuel conversion at higher temperature. However, excessive temperature possibly strengthens the thermodynamic limitation and also increases the risk of sintering. Taking these two sides as well as economic cost into consideration, the temperature should be controlled in a reasonable range. In addition, the reduction phase, $CaFe_3O_5$, is also found to own moderate catalytic activity, which is not surprising because Fe_3O_4 had been proved to have the catalytic ability for the WGS reaction at high temperature [57]. Note that the addition of CaO intensifies the catalytic activity, and is also favorable for the sintering-resistance.

Different from the OCs' catalytic effect on the WGS reaction, the iron-containing substances with low oxygen potential (*e.g.*, the reduced iron oxide and calcium ferrites) act as reactants in the steam-iron reaction. Therefore, the reduction ability of iron-containing phases is closely correlated with the H_2 yield. While the forming $Ca_2Fe_2O_5$ possesses bad reduction ability thermodynamically, which will definitely limit the H_2 yield. Nevertheless, from the analysis in Section 3.3.2, $Ca_2Fe_2O_5$ plays an active role in the hydrogen production rate, which is attributed to active sites provided by $Ca_2Fe_2O_5$. However, the mechanism is still not clear, which is worth further pursuing. Taking both the H_2 yield and H_2 production rate into consideration, the molar ratio of CaO to Fe_2O_3 should be controlled at 0.2:0.8.

Generally, the effect of the bimetallic Ca—Fe based OCs on the hydrogen productivity is four-fold. (1) active lattice oxygen provided by the OCs may combust H_2 from coal pyrolysis / char gasification, leading to the decrease of H_2 yield in the initial stage of coal/char conversion; (2) catalytic substance (*e.g.*, $CaFe_2O_5$) in the partially reduced OC particles may enhance char gasification, generating more H_2 in the latter stage; (3) the partially reduced OCs will catalyze the WGS reaction, and more CaO addition contributes the elevation of CO conversion, subsequently resulting in a higher H_2 yield; (4) the deeply reduced OCs containing metallic iron or low-valent iron oxides can be oxidized by steam to generate H_2, where dre-FeCa0 and dre-FeCa20 can acquire higher H2 yield compared to dre-FeCa50 and dre-FeCa70. As a comprehensive result, the H_2 yield is generally elevated as the increase of CaO addition. There is an exception for FeCa50 in the char CLG test (Fig. 7), which may be ascribed to its excellent lattice oxygen donation ability and quite large total oxygen loss percentage (Table 4), consuming more combustible gases like H_2.

Generally, the H_2/CO ratio increases as the content of CaO in both coal and char CLG tests (Figs. 4 and 7). However, FeCa70 with the highest CaO content shows negative effect on the H_2/CO ratio, which may be due to the least oxygen loss amount (Table 4) for this kind of Ca—Fe based OC.

4. Conclusion

In this work, calcium ferrites, prepared by the wet-impregnation method, are chosen as oxygen carriers (OCs) in the coal-derived CLG process. Both the promoting and regulating effects of these CaO/Fe_2O_3 OCs are investigated detailedly, using coal (char) as fuels.

The coal CLG results indicate that increasing CaO addition can elevate the gas LHV, which is attributed to less syngas consumption with the decrease of active content. The maximum H_2/CO ratio of 4.6 is achieved as well as 1.4 Nm^3 syngas /kg coal is yielded in FeCa50. During this process the gasification inhibitation and catalytic contribution may co-exist.

Subsequently, the gas distribution and evolution are further investigated using coal char as fuel. It is found that stronger combustion reactions are accompanied in the initial gasification stage. And the FeCa50 can achieve the maximum oxygen loss rate of 1.2×10^{-3} g/s owing to its excellent oxygen donation ability. The total gas distribution suggests that the rich active oxygen favors fuel gas combustion, in other words, FeCa0 tends to obtain the lowest syngas yield. Note that the highest H_2/CO ratio is also achieved in the presence of FeCa50, which is same as the coal-derived CLG test, and this implies that FeCa50 has an advantage for hydrogen production. In addition, by analysis of the (instantaneous) rate of carbon conversion based on all fresh and reduced samples, $Ca_2Fe_2O_5$ is deduced to be the catalytic substance. Nevertheless, the catalytic effect is prominent at the later stage of char gasification. And the initial contribution relies more on active oxygen release.

The WGS experiments indicate that the catalytic activity of partially re-OCs is elevated with the increases of reaction temperature from 600 to 800 °C. Moreover, increasing CaO content also contributes the elevation of CO conversion, and the CO conversion can attain the highest value of 77% for re-FeCa70 at 800 °C. Additionally, increasing CaO content and elevating reaction temperature can both help improve the selectivity of R4. The order of catalytic activity to the WGS reaction based on CO conversion and selectivity can be both determined as $Ca_2Fe_2O_5$ (strong), $CaFe_3O_5$ (moderate) and Fe_3O_4 (weak).

The experimental results based on the steam-iron reaction indicate that the deeply reduced FeCa0 and FeCa20 OCs (dre-FeCa0 and dre-FeCa20) can acquire higher H_2 yield compared to dre-FeCa50 and dre-FeCa70. While dre-FeCa20 and dre-FeCa50 can obtain higher rate peaks than dre-FeCa70 and dre-FeCa0. Additionally, $Ca_2Fe_2O_5$ is validated to promote the hydrogen production rate.

Acknowledgments

This work was supported by the National Key R&D Program of China (2018YFB0605402). The authors are grateful to the Analytical and Testing Center of HUST for XRD and SEM-EDX measurements.

References

[1] J.M. Zeng, R. Xiao, D.W. Zeng, Y. Zhao, H.Y. Zhang, D.K. Shen, High H_2/CO-ratio syngas production from chemical looping gasification of sawdust in a dual fluidized bed gasifier, Energy Fuel 30 (2016) 1764–1770.

[2] H.-C. Wu, Y. Ku, Chemical looping gasification of charcoal with iron-based oxygen carriers in an annular dual-tube moving bed reactor, Aerosol Air Qual. Res. 16 (2016) 1093–1103.

[3] H. Ding, Y. Xu, C. Luo, Y. Zheng, Q. Shen, Z. Liu, L. Zhang, Synthesis and characteristics of BaSrCoFe-based perovskite as a functional material for chemical looping gasification of coal, Int. J. Hydrog. Energy 41 (2016) 22846–22855.

[4] J. Adánez, L.F. de Diego, F. García-Labiano, P. Gayán, A. Abad, Selection of oxygen carriers for chemical-looping combustion, Energy Fuel 18 (2004) 371–377.

[5] F.X. Li, H.R. Kim, D. Sridhar, F. Wang, L. Zeng, J. Chen, L.S. Fan, Syngas chemical looping gasification process: oxygen carrier particle selection and performance, Energy Fuel 23 (2009) 4182–4189.

[6] S. Luo, L. Zeng, L.S. Fan, Chemical looping technology: oxygen carrier characteristics, Annu. Rev. Chem. Biomol. Eng. 6 (2015) 53–75.

[7] Z. Huang, Y. Zhang, J. Fu, L. Yu, M. Chen, S. Liu, F. He, D. Chen, G. Wei, K. Zhao, A. Zheng, Z. Zhao, H. Li, Chemical looping gasification of biomass char using iron ore as an oxygen carrier, Int. J. Hydrog. Energy 41 (2016) 17871–17883.

[8] Z. Huang, F. He, H. Zhu, D. Chen, K. Zhao, G. Wei, Y. Feng, A. Zheng, Z. Zhao, H. Li, Thermodynamic analysis and thermogravimetric investigation on chemical looping gasification of biomass char under different atmospheres with Fe_2O_3 oxygen carrier, Appl. Energy 157 (2015) 546–553.

[9] M.A. San Pio, M. Martini, F. Gallucci, I. Roghair, M. van Sint Annaland, Kinetics of CuO/SiO_2 and CuO/Al_2O_3 oxygen carriers for chemical looping combustion, Chem. Eng. Sci. 175 (2018) 56–71.

[10] A. Abad, P. Gayán, F. García-Labiano, L.F. de Diego, J. Adánez, Relevance of plant design on CLC process performance using a Cu-based oxygen carrier, Fuel Process. Technol. 171 (2018) 78–88.

[11] J.A. Medrano, H.P. Hamers, G. Williams, M. van Sint Annaland, F. Gallucci, NiO/$CaAl_2O_4$ as active oxygen carrier for low temperature chemical looping applications, Appl. Energy 158 (2015) 86–96.

[12] L.F. de Diego, M. Ortiz, F. García-Labiano, J. Adánez, A. Abad, P. Gayán, Hydrogen production by chemical-looping reforming in a circulating fluidized bed reactor using Ni-based oxygen carriers, J. Power Sources 192 (2009) 27–34.

[13] G. Azimi, H. Leion, T. Mattisson, A. Lyngfelt, Chemical-looping with oxygen uncoupling using combined Mn-Fe oxides, testing in batch fluidized bed, Energy Procedia 4 (2011) 370–377.

[14] S. Sundqvist, T. Mattisson, H. Leion, A. Lyngfelt, Oxygen release from manganese ores relevant for chemical looping with oxygen uncoupling conditions, Fuel 232 (2018) 693–703.

[15] M. Aghabararnejad, G.S. Patience, J. Chaouki, TGA and kinetic modelling of Co, Mn and Cu oxides for chemical looping gasification (CLG), Can. J. Chem. Eng. 92 (2014) 1903–1910.

[16] M. Aghabararnejad, G.S. Patience, J. Chaouki, Transient modeling of biomass steam gasification with Co_3O_4, Fuel 140 (2015) 354–364.

[17] M.M. Sarafraz, M. Jafarian, M. Arjomandi, G.J. Nathan, Potential use of liquid metal oxides for chemical looping gasification: a thermodynamic assessment, Appl. Energy 195 (2017) 702–712.

[18] M.M. Sarafraz, M. Jafarian, M. Arjomandi, G.J. Nathan, Potential of molten lead oxide for liquid chemical looping gasification (LCLG): a thermochemical analysis, Int. J. Hydrog. Energy 43 (2018) 4195–4210.

[19] B. Wang, R. Yan, H. Zhao, Y. Zheng, Z. Liu, C. Zheng, Investigation of chemical looping combustion of coal with $CuFe_2O_4$ oxygen carrier, Energy Fuel 25 (2011) 3344–3354.

[20] P. Niu, Y. Ma, X. Tian, J. Ma, H. Zhao, Chemical looping gasification of biomass: part I. screening Cu-Fe metal oxides as oxygen carrier and optimizing experimental conditions, Biomass Bioenergy 108 (2018) 146–156.

[21] X. Tian, P. Niu, Y. Ma, H. Zhao, Chemical-looping gasification of biomass: part II. Tar yields and distributions, Biomass Bioenergy 108 (2018) 178–189.

[22] Z. Yu, C. Li, X. Jing, Q. Zhang, Z. Wang, Y. Fang, J. Huang, Catalytic chemical looping combustion of carbon with an iron-based oxygen carrier modified by K_2CO_3: catalytic mechanism and multicycle tests, Fuel Process. Technol. 135 (2015) 119–124.

[23] Q. Guo, Y. Liu, W. Jia, M. Yang, X. Hu, H.-J. Ryu, Performance of Ca-based oxygen carriers decorated by K_2CO_3 or Fe_2O_3 for coal chemical looping combustion, Energy Fuel 28 (2014) 7053–7060.

[24] L. Chen, J. Bao, L. Kong, M. Combs, H.S. Nikolic, Z. Fan, K. Liu, Activation of ilmenite as an oxygen carrier for solid-fueled chemical looping combustion, Appl. Energy 197 (2017) 40–51.

[25] J. Bao, Z. Li, N. Cai, Promoting the reduction reactivity of ilmenite by introducing foreign ions in chemical looping combustion, Ind. Eng. Chem. Res. 52 (2013) 6119–6128.

[26] L. Chen, L. Yang, F. Liu, H. Nikolic, Z. Fan, K. Liu, Evaluation of multi-functional iron-based carrier from bauxite residual for H_2-rich syngas production via chemical-looping gasification, Fuel Process. Technol. 156 (2017) 185–194.

[27] G. Deng, K. Li, Z. Gu, X. Zhu, Y. Wei, X. Cheng, H. Wang, Synergy effects of combined red muds as oxygen carriers for chemical looping combustion of methane, Chem. Eng. J. 341 (2018) 588–600.

[28] J. Udomsirichakorn, P.A. Salam, Review of hydrogen-enriched gas production from stream gasification of biomass: the prospect of CaO-based chemical looping gasification, Renew. Sust. Energ. Rev. 30 (2014) 565–579.

[29] Q. Guo, Y. Cheng, Y. Liu, W. Jia, H.-J. Ryu, Coal chemical looping gasification for syngas generation using an iron-based oxygen carrier, Ind. Eng. Chem. Res. 53 (2014) 78–86.

[30] M. Ismail, W. Liu, S.A. Scott, The performance of Fe_2O_3-CaO oxygen carriers and the interaction of iron oxides with CaO during chemical looping combustion and H_2 production, Energy Procedia 63 (2014) 87–97.

[31] M. Ismail, W. Liu, M.T. Dunstan, S.A. Scott, Development and performance of iron based oxygen carriers containing calcium ferrites for chemical looping combustion and production of hydrogen, Int. J. Hydrog. Energy 41 (2016) 4073–4084.

[32] R. Siriwardane, J. Riley, H. Tian, G. Richards, Chemical looping coal gasification with calcium ferrite and barium ferrite via solid-solid reactions, Appl. Energy 165 (2016) 952–966.

[33] J. Zhang, T. He, Z. Wang, M. Zhu, K. Zhang, B. Li, J. Wu, The search of proper oxygen carriers for chemical looping partial oxidation of carbon, Appl. Energy 190 (2017) 1119–1125.

[34] I. Zamboni, C. Courson, A. Kiennemann, Fe-Ca interactions in Fe-based/CaO catalyst/sorbent for CO_2 sorption and hydrogen production from toluene steam reforming, Appl. Catal. B Environ. 203 (2017) 154–165.

[35] M. Keller, H. Leion, T. Mattisson, A. Lyngfelt, Gasification inhibition in chemical-looping combustion with solid fuels, Combust. Flame 158 (2011) 393–400.

[36] A. Cuadrat, A. Abad, L.F. de Diego, F. García-Labiano, P. Gayán, J. Adánez, Prompt considerations on the design of chemical-looping combustion of coal from experimental tests, Fuel 97 (2012) 219–232.

[37] S. Luo, L. Barrio, T.D. Nguyen-Phan, D. Vovchok, A.C. Johnston-Peck, W. Xu, E.A. Stach, J.A. Rodriguez, S.D. Senanayake, Importance of low dimensional CeO_x nanostructures in Pt/CeO_x-TiO_2 catalysts for the water-gas shift reaction, J. Phys. Chem. C 121 (2017) 6635–6642.

[38] A.S. Duke, K. Xie, A.J. Brandt, T.D. Maddumapatabandi, S.C. Ammal, A. Heyden, J.R. Monnier, D.A. Chen, Understanding active sites in the water-gas shift reaction for Pt-Re catalysts on titania, ACS Catal. 7 (2017) 2597–2606.

[39] T.M. Kokumai, D.A. Cantane, G.T. Melo, L.B. Paulucci, D. Zanchet, VO_x-Pt/Al_2O_3 catalysts for hydrogen production, Catal. Today 289 (2017) 249–257.

[40] J.H. Lin, P. Biswas, V.V. Guliants, S. Misture, Hydrogen production by water-gas shift reaction over bimetallic Cu-Ni catalysts supported on La-doped mesoporous ceria, Appl. Catal. A Gen. 387 (2010) 87–94.

[41] S.C. Ammal, A. Heyden, Origin of the unique activity of Pt/TiO_2 catalysts for the water-gas shift reaction, J. Catal. 306 (2013) 78–90.

[42] J. Yu, F.-J. Tian, L.J. Mckenzie, C.-Z. Li, Char-supported nano iron catalyst for water-gas-shift reaction: hydrogen production from coal/biomass gasification, Process. Saf. Environ. Prot. 84 (2006) 125–130.

[43] G.K. Boreskov, Forms of oxygen bonds on the surface of oxidation catalysts, Discuss. Faraday Soc. 41 (1966) 263–276.

[44] G.K. Boreskov, T.M. Yur'eva, A.S. Sergeeva, Mechanism of the conversion of carbon monoxide on an iron-chromium catalyst, Kinet. Katal. 11 (1970) 1476–1478.

[45] A. Haryanto, S.D. Fernando, S.D.F. To, P.H. Steele, L. Pordesimo, S. Adhikari, Hydrogen production through the water-gas shift reaction: thermodynamic equilibrium versus experimental results over supported Ni catalysts, Energy Fuel 23 (2009) 3097–3102.

[46] H. Song, U.S. Ozkan, Changing the oxygen mobility in Co/Ceria catalysts by Ca incorporation: implications for ethanol steam reforming, J. Phys. Chem. A 114 (2010) 3796–3801.

[47] Z. Fu, J. Wang, N. Zhang, Y. An, Z. Yang, Effect of Cu doping on the catalytic activity of Fe_3O_4 in water-gas shift reactions, Int. J. Hydrog. Energy 40 (2015) 2193–2198.

[48] Y. Tanaka, T. Iizuka, Methanation of carbon monoxide with water over supported rhodium catalysts, Aust. J. Chem. 38 (1985) 293–296.

[49] A.P. Il'in, N.N. Smirnov, A.A. Il'in, Mechanochemical synthesis of calcium and copper ferrite catalysts for medium-temperature carbon monoxide conversion, Kinet. Catal. 47 (2006) 901–906.

[50] E.R. Monazam, R. Siriwardane, Hydrogen production by steam oxidation of reduced $CaFe_2O_4$ during chemical looping coal gasification: equilibrium and kinetic analysis, Energy Fuel 32 (2018) 10398–10407.

[51] C.B. Vanpeteghem, R.J. Angel, J. Zhao, N.L. Ross, G.J. Redhammer, F. Seifert, The effect of oxygen vacancies and aluminium substitution on the high-pressure properties of brownmillerite-structured Ca_2Fe_{2-x} Al_xO_5, Phys. Chem. Miner. 35 (2008) 493–504.

[52] J. Berggren, Refinement of the crystal structure of dicalcium ferrite, $Ca_2Fe_2O_5$, Acta, Chem. Scand. 25 (1971) 3616–3624.

[53] J.C. Grenier, M. Pouchard, P. Hagenmuller, Vacancy ordering in oxygen-deficient perovskite-related ferrites, Struct. Bond. 47 (1981) 1–25.

[54] N.L. Ross, R.J. Angel, F. Seifert, Compressibility of brownmillerite ($Ca_2Fe_2O_5$): effect of vacancies on the elastic properties of perovskites, Phys. Earth Planet. Inter. 129 (2002) 145–151.

[55] L.A. Isupova, S.V. Tsybulya, G.N. Kryukova, A.A. Budneva, E.A. Paukshtis, G.S. Litvak, V.P. Ivanov, V.N. Kolomiichuk, Yu.T. Pavlyukhin, V.A. Sadykov, Mechanochemical synthesis and catalytic properties of the calcium ferrite $Ca_2Fe_2O_5$, Kinet. Catal. 43 (2002) 122–128.

[56] D. Hirabayashi, T. Yoshikawa, K. Mochizuki, K. Suzuki, Y. Sakai, Formation of brownmillerite type calcium ferrite ($Ca_2Fe_2O_5$) and catalytic properties in propylene combustion, Catal. Lett. 110 (2006) 155–160.

[57] C. Ratnasamy, J.P. Wagner, Water gas shift catalysis, Catal. Rev. 51 (2009) 325–440.